CrystEngComm

ROYAL SOCIETY OF CHEMISTRY

PAPER

Cite this: *CrystEngComm*, 2021, **23**, 2854

Structural, magnetic and Mössbauer spectroscopic studies of the $[Fe(3\text{-bpp})_2](CF_3COO)_2$ complex: role of crystal packing leading to an incomplete Fe(II) high spin ⇌ low spin transition†

Kristian Handoyo Sugiyarto, [a] Djulia Onggo, [b] Hiroki Akutsu, [c] Varimalla Raghavendra Reddy, [d] Hari Sutrisno, [a] Yasuhiro Nakazawa [c] and Ashis Bhattacharjee *[e]

Received 19th November 2020,
Accepted 1st March 2021

DOI: 10.1039/d0ce01687j

rsc.li/crystengcomm

Single crystal X-ray diffraction, magnetic and ^{57}Fe Mössbauer spectroscopic studies of a new iron(II)-based spin transition complex – $[Fe(3\text{-bpp})_2](CF_3COO)_2$ (bpp = 2,6-bis(pyrazol-3-yl)pyridine) are reported. The complex exhibits an incomplete thermal high spin (HS) ⇌ low spin (LS) transition at ~226 K which is not associated with any crystallographic transition. Only one of the two crystallographic iron(II) sites undergoes the spin transition, while the other HS site remains invariant of temperature down to 10 K. The origin of the incomplete spin transition is understood by analysing the nature of crystal packing below and above the transition temperature with special attention to the degree of distortion. The present study shows the role of the degree of distortion associated with the cations in the $[Fe(3\text{-bpp})_2]^{2+}$ spin transition complexes.

Introduction

Though known for decades, iron(II) high spin (HS, $^5T_2$, $S = 2$) ⇌ low spin (LS, $^1A_1$, $S = 0$) transition (ST) materials[1,2] continuously draw research interest from both fundamental and applied disciplines.[3–9] These materials reversibly switch their spin state under the influence of temperature, pressure and irradiation with light. In the solid state, cooperative interactions between spin-changing molecules influence the nature of the spin transition process. Generally, cooperativity originates from the difference in the metal–donor atom bond lengths in two different spin states, where the solid lattice provides the communication mechanism between the different spin sites. Besides the bridging ligands' important role in influencing this mechanism,[10] the hydrogen bonding interactions also significantly modulate the cooperativity and hence, influence the nature of spin transition.[11,12]

One extensively studied and flexible spin transition system, where hydrogen bonding strongly influences the cooperativity, is the $[Fe(3\text{-bpp})_2]^{2+}$ family of complexes (bpp = 2,6-bis(pyrazol-3-yl) pyridine). Goodwin and his co-workers synthesized a large number of $[Fe(3\text{-bpp})_2]X_2{\cdot}nH_2O$ spin transition complexes (X = NO_3, Br, I, ClO_4, BF_4, PF_6, CF_3SO_3, NCS, NCSe, and X_2 = $[Fe(CN)_5(NO)]$) and explored their magneto-structural correlations.[13–21] It is this system which is hydrogen bonded to associate anions and/or solvate molecules present in the solid, and this interaction is the medium of propagation of the cooperativity of spin transition.[22] This spin transition system provides huge flexibility in synthetic and structural chemistry,[23] and this is why the $[Fe(3\text{-bpp})_2]^{2+}$ system still draws large research interest[22–29] in the search of spin transition materials with application potential.

In this light, as trifluoroacetate is considered to be a suitable monovalent counteranion,[30] we have synthesized a new complex of this family – $[Fe(3\text{-bpp})_2](CF_3COO)_2$, **1**. In the present paper, we report the crystal structure of this complex and its spin transition properties are revealed with the help of temperature-dependent magnetic and Mössbauer spectroscopic studies. The complex exhibits an incomplete (HS + HS) ⇌ (HS + LS) transition at ~226 K which has been understood by an in-depth analysis of the crystal structure above and below the spin transition temperature taking into account the degree of distortion.

Results and discussion

Crystal structure of $[Fe(3\text{-bpp})_2](CF_3COO)_2$, 1

Single crystal X-ray diffraction patterns of **1** were obtained at 300, 250, 200 and 100 K, and the estimated crystal

[a] *Department of Chemistry Education, Yogyakarta State University, Indonesia*
[b] *Inorganic and Physical Chemistry Research Division, Institut Teknologi, Bandung, Indonesia*
[c] *Graduate School of Science, Osaka University, Toyonaka, Osaka, Japan*
[d] *IUC DAE CSR, Indore Campus, Indore, India*
[e] *Department of Physics, Visva-Bharati University, Santiniketan, India. E-mail: ashis.bhattacharjee@visva-bharati.ac.in*

† Electronic supplementary information (ESI) available: Supplementary figures (S1–S5) and CIFs. CCDC 2031403, 2031405, 2061474 and 2061475. For ESI and crystallographic data in CIF or other electronic format see DOI: 10.1039/d0ce01687j

parameters are compared in Table 1. Fig. 1 shows the asymmetric unit of **1** at 300 K with the atom numbering scheme where two halves of the divalent cations (Cation1 and Cation2) of Fe(3-bpp)$_2$ and two monovalent anions of CF_3COO^- are crystallographically independent. The crystallographically independent part of Cation1 has one ligand (bpp1 in Fig. 2) and one iron atom (Fe1). Fe1 is located on a two-fold axis, the symmetry operation of which generates another ligand on Fe1 to form Fe(3-bpp)$_2$. The dihedral angle between the two bpp ligands in a molecule is observed to be 69.32°. The asymmetric part of Cation2 has two halves of the ligands (bpp2 and bpp3 in Fig. 2) and an iron atom (Fe2). Fe2 along with C18, N9, N6, and C12 are located on a two-fold axis, the operation of which generates the other two halves of ligands to form Fe(3-bpp)$_2$. The crystal structure at 300 K is shown in Fig. 2. The dihedral angle between the bpp ligands of Cation2 is calculated as 83.98°, suggesting that Cation1 is more distorted from ideal octahedral coordination than that of Cation2 (see θ values in Table 2). Four crystallographically independent N–H groups of the bpp ligands are connected with four independent O atoms of the carboxylic groups of the two independent anions *via* relatively short hydrogen bonds (see Table 2). Each anion is bridged between Cation1 and Cation2 to form a strong 3D hydrogen bond network. There are two crystallographically independent CF_3COO^- anions, both $-CF_3$ groups of which are disordered as shown in Fig. 1, where each anion has six partially occupied F atoms whose total occupancy is 3. Relatively large thermal ellipsoids of F atoms of both anions indicate that the $-CF_3$ rotation exists at 300 K.

Upon solving the crystal structure of **1** at 250, 200 and 100 K, it is found that the space group (*C*2/*c*) and the cell

Table 1 Crystal data for compound **1**

Temperature	300 K	250 K	200 K	100 K
Composition	[Fe(3-bpp)$_2$](CF$_3$COO)$_2$			
Formula	$C_{26}H_{18}O_4N_{10}F_6Fe$			
Fw	704.33			
Space group	*C*2/*c*	*C*2/*c*	*C*2/*c*	*C*2/*c*
a (Å)	19.4312(8)	19.3817(6)	19.2114(7)	19.2154(4)
b (Å)	21.9435(8)	21.9198(7)	21.9406(9)	21.7934(4)
c (Å)	14.1557(7)	14.0784(5)	13.9778(5)	13.8564(4)
β (°)	92.787(7)	92.693(3)	92.151(3)	92.334(7)
V (Å^3)	6028.7(4)	5974.5(3)	5887.6(4)	5797.8(2)
Z	8	8	8	8
d_{calc} (g cm^{-1})	1.552	1.566	1.589	1.614
μ (cm^{-1})	5.880	5.933	6.021	6.114
F(000)	2848	2848	2848	2848
2θ range (°)	4–55	4–55	4–55	4–55
Total ref.	28 828	21 549	19 363	27 656
Unique ref.	6880	6744	6668	6595
R_{int}	0.0331	0.0216	0.0335	0.0340
Parameters	447	447	437	437
R_1 ($I > 2\sigma(I)$)	0.046	0.043	0.044	0.039
wR_2 (all data)	0.128	0.125	0.126	0.093
S	1.025	1.066	1.070	1.072
$\Delta\rho_{max}$ (e Å^{-3})	0.44	0.51	0.81	0.63
$\Delta\rho_{min}$ (e Å^{-3})	−0.58	−0.63	−0.57	−0.58
Machines	Rapid Auto	XtaLAB	XtaLAB	Rapid Auto
CCDC	2031403	2061475	2061474	2031405

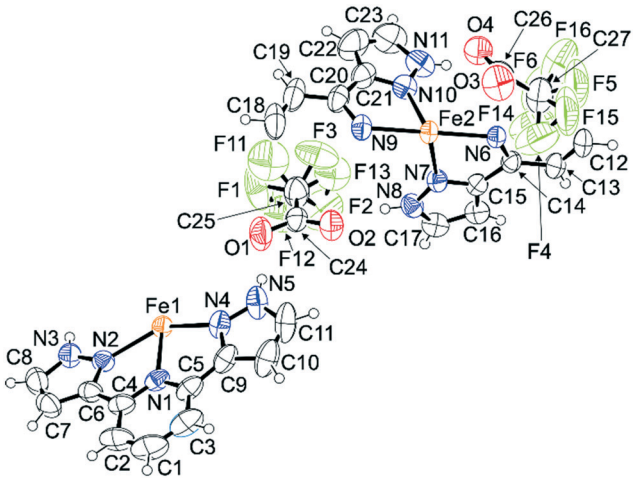

Fig. 1 ORTEP diagram of the asymmetric unit of **1** at 300 K with the atom numbering scheme.

parameters are similar to those obtained at 300 K. This indicates that no structural phase transition occurs in **1** in the 300–100 K range. Fig. 3 shows the 3D hydrogen bond network in **1** at 100 K. At this temperature, the intramolecular ligand–ligand dihedral angles of Cation1 and Cation2 are 66.61° and 81.03°, respectively, and these values are similar to those obtained at 300 K. The N–H···O hydrogen bonds between the cation and anion at 100 K (see Table 2) are not significantly different from those at 300 K (Fig. S1†). A strong difference between the structures of **1** at 100 K and 300 K is observed in the Fe–N distances. The Fe–N distances of Cation1 are almost same at 300, 250, 200 and 100 K, the average Fe–N distances being 2.1709(19), 2.1682(17), 2.1715(18) and 2.1741(16) Å, respectively. These values indicate that Cation1 is in the HS state from 300 K down to 100 K.[31] On the other hand, the Fe–N distances of Cation2 are different at different temperatures, especially at 250 K

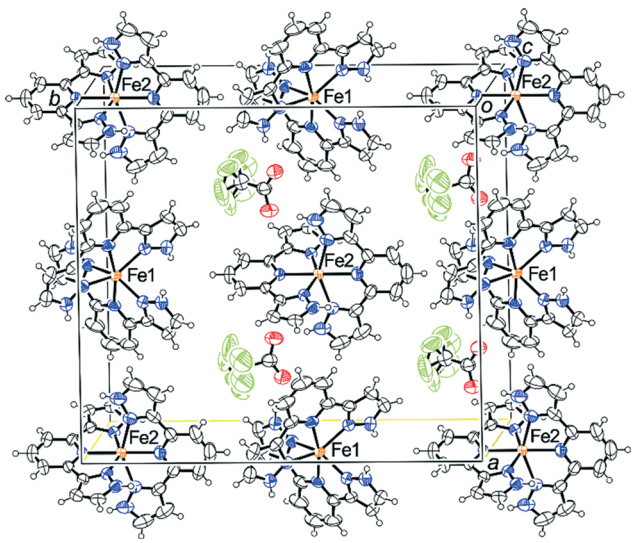

Fig. 2 Crystal structure of **1** at 300 K.

Table 2 Selected bond and hydrogen bond lengths (Å) for **1** estimated at different temperatures

	300 K	250 K	200 K	100 K
Fe1–N1	2.1297(18)	2.1322(16)	2.1360(17)	2.1394(15)
Fe1–N2	2.193(2)	2.1906(18)	2.1965(18)	2.2017(16)
Fe1–N4	2.190(2)	2.1819(18)	2.1821(18)	2.1810(16)
Fe2–N6	2.123(2)	2.095(2)	1.935(2)	1.931(2)
Fe2–N7	2.1624(19)	2.1372(17)	1.9817(16)	1.9742(15)
Fe2–N9	2.124(3)	2.104(2)	1.930(2)	1.927(2)
Fe2–N10	2.193(2)	2.1667(18)	1.9825(17)	1.9764(15)
N3···O4	2.759(3)	2.750(3)	2.739(2)	2.730(2)
N5···O1	2.668(3)	2.663(3)	2.676(3)	2.675(2)
N8···O2	2.731(3)	2.723(2)	2.701(2)	2.695(2)
N11···O3	2.693(4)	2.690(4)	2.689(3)	2.703(2)

and 200 K. The average Fe–N distance at 200 K is 1.9656(19) Å, which is similar to that at 100 K (1.9600(15) Å), but is shorter than that at 250 K (2.1345(19) Å) and at 300 K (2.160(2) Å) by 0.17 Å and 0.19 Å, respectively. This definitely indicates that Cation2 is in the HS state at 300 and 250 K, and is in the LS state at 200 and 100 K, while Cation1 remains in the HS state down to 100 K. Thus, the structural data analysis indicates that complex **1** undergoes a thermal HS ⇌ LS transition of Fe(II). As shown in Fig. 3, at 100 K, a crystallographically independent anion (Anion1, consisting of C25–26, O1–2 and F1–3) has an ordered $-CF_3$ group and the other anion (Anion2, consisting of C27–28, O3–4, F4–6 and F14–16) has a disordered $-CF_3$ group. We guess that the rotation of Anion1 definitely stops at least at 100 K. The rotation of Anion2 also stops at 100 K with positional disorder. In addition, two crystallographically dependent Anion1 molecules (x, y, z and $1-x$, y, $3/2-x$) sandwich the bpp3 ligand of Cation2 as shown in Fig. S2,† whilst Anion2 is surrounded by both Cation1 and Cation2.

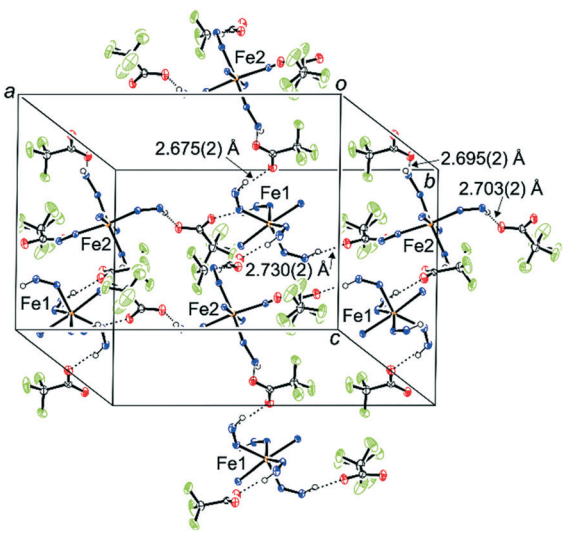

Fig. 3 3D hydrogen bond network of **1** at 100 K, where all carbon and hydrogen atoms of the bpp ligands are omitted for clarity.

Magnetic properties

Experimentally measured magnetic data for **1** obtained under ambient pressure and a 10 kOe magnetic field in the 10–300 K range in a cooling–heating cycle were converted to molar magnetic susceptibility $\chi_M(T)$ data. Fig. 4(a) shows the $\chi_M T$ *vs.* T plots obtained using cooling and heating protocols. At 300 K the $\chi_M T$ has a value of 3.46 emu mol^{-1} K, which is close to that expected for an isolated HS hexacoordinated Fe(II) ion with $S = 2$ and $g = 2$.[19,32] The $\chi_M T$ value decreases very slowly when the temperature is lowered from 300 K down to 250 K and below this temperature, it undergoes a gradual decrease to a plateau of *ca.* 1.78 emu mol^{-1} K at *ca.* 180 K indicating a gradual but incomplete thermal (HS + HS) ⇆ (HS + LS) transition of Fe(II) in **1**. With further lowering of temperature, the $\chi_M T$ value exhibits a wide plateau down to 30 K. Below 30 K the $\chi_M T$ value decreases owing to the zero-field-splitting (ZFS) effect in the remaining HS fraction of Fe(II) and reaches $\chi_M T$ = 1.76 emu mol^{-1} K at 10 K.[33,34] When the sample is heated above 10 K, the $\chi_M T(T)$ plot retraces almost the same path as observed while cooling indicating no hysteresis. The (HS + HS) ⇌ (HS + LS) transition temperature $T_{1/2}$ (average) is ~226 K, measured from the maximum of the $d(\chi_M T)/dT$ *vs.* T plots (inset in Fig. 4a).

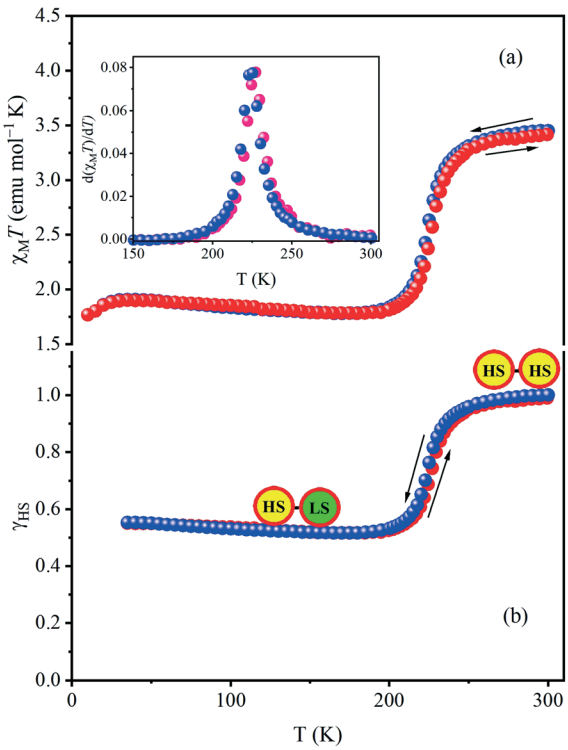

Fig. 4 (a) Variation of χ_MT with temperature for **1** during cooling and heating under a 10 kOe magnetic field. Inset shows the variation of $\frac{d(\chi_M T)}{dT}$ *vs.* T plot. (b) Variation of the high spin fraction (γ_{HS}) obtained using eqn (1) with temperature for **1** during cooling and heating. Arrows are a guide to the eye. The $\gamma_{HS}(T)$ data obtained from the $\chi_M T$ data below *ca.* 30 K reflect the effect of zero-field splitting and are, thus, omitted.

The molar high spin fraction γ_{HS} is evaluated from the estimated $\chi_M(T)$ data for **1** by application of the following relationship:[19]

$$\gamma_{HS}(T) = \frac{(\chi_M T)_{observed}(T) - (\chi_M T)_{LS}}{(\chi_M T)_{HS}(T) - (\chi_M T)_{LS}}. \quad (1)$$

The value of $(\chi_M T)_{HS}$ is calculated using the spin only effective magnetic moment value for high spin Fe(II) [$\mu_{eff} = \sqrt{(8\chi_M T)} = 2\sqrt{S(S+1)}$, where S = 2 for high spin Fe(II)] and the $(\chi_M T)_{LS}$ value is taken to be 2×10^{-4} emu mol^{-1} K.[35] The temperature dependence of γ_{HS} estimated using cooling and heating protocols for the 10–300 K range is shown in Fig. 4(b) which confirms that complex **1** undergoes a half-spin transition [(HS + HS) ⇌ (HS + LS)] of Fe(II). The value of γ_{HS} at 300 K is 0.99 whereas in the 180 K to 30 K plateau γ_{HS} ranges between 0.55 and 0.51. The γ_{HS} *vs.* T plot shows that both HS and LS Fe(II) states are present at ~1 : 1 ratio in the 180–30 K range, and this gives rise to the plateau region observed in the $\chi_M T$ *vs.* T plot. The TG-DTA study confirmed the thermal stability of **1** in the working range of temperature (Fig. S3†). Thus, the cooling and heating processes during the magnetic studies do not lead to any loss of solvent molecules affecting the nature of spin transition as reported for $[Fe(3\text{-bpp})_2](NCS)_2 \cdot 2H_2O$.[19] Further, as suggested by the variable temperature crystal structure analysis, the magnetic observations also lead to the fact that only Fe(2) species associated with Cation2 change the spin state from HS to LS during cooling from 300 K under ambient pressure and *vice versa*, while the [Fe(1)N_6] coordination environment is quite rigidly maintained in the HS state for the whole range of working temperatures.

Mössbauer spectroscopy of 1

The Mössbauer spectrum of **1** was recorded at two different temperatures 300 and 100 K (Fig. 5). Mössbauer spectra at 300 K were resolved into two doublets of equal areal intensity (~48%). These doublets can be characterized by the quadrupole splitting, E_Q = 2.22(0.01) mm s^{-1}, and isomer shift, δ = 0.95(0.01) mm s^{-1} (relative to α-iron), and E_Q = 2.46(0.01) mm s^{-1} and isomer shift, δ = 0.99(0.02) mm s^{-1} (relative to α-iron), respectively, where both doublets correspond to the HS (S = 2) ground state of Fe(II). Contribution from a small singlet (areal intensity = ~4%) with δ = 0.32 mm s^{-1} was evident in this spectrum and this may be due to iron(III) impurities present.[36] The powder X-ray diffraction (PXRD) pattern of the bulk sample is compared with the calculated result obtained using the 300 K single crystal X-ray diffraction data in Fig. S4† where both spectra matched perfectly well and no extra peak in the PXRD pattern is noticed. This suggests that the impurity present in **1**, if any, is negligible which is in consistent with the observation made from the Mössbauer spectroscopic study.

With lowering of the temperature of the sample to 100 K, a doublet due to Fe(II) HS appears with E_Q = 3.23(0.01) mm s^{-1} and δ = 1.08(0.01) mm s^{-1} along with another doublet

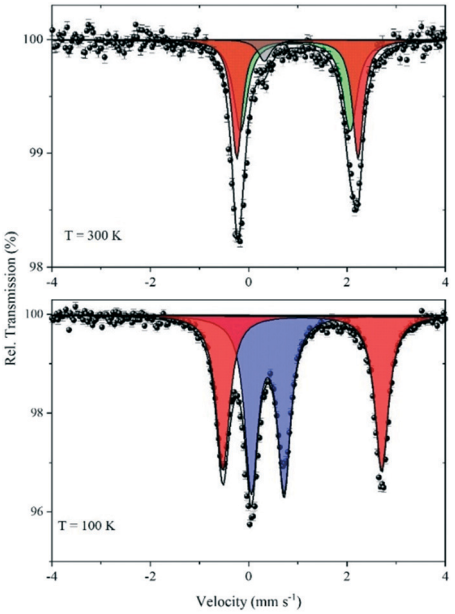

Fig. 5 Mössbauer spectra of **1** obtained at two different temperatures – above and below the spin transition temperature.

with E_Q = 0.67(0.01) mm s^{-1} and δ = 0.39(0.01) mm s^{-1} due to Fe(II) LS.[19] The ratio of the areal intensity of the HS and LS doublets observed at 100 K is *ca.* 1 : 1. Thus, the Fe(II) doublets observed at 300 K change their position significantly. At this point, it may be noted that, in general, a more positive isomer shift value implies a reduction in the s-electron density which reflects an increase in the Fe(II)–N bond length, and an increment of the quadrupole splitting may indicate an enhancement in the intra-ligand distortion of the HS Fe(II) complex.[37] It is interesting to note that the Mössbauer spectroscopic study identifies two distinguishable Fe(II) HS sites in **1** at 300 K. With lowering of the temperature, one of those Fe(II) (*i.e.*, Fe(2) from structural analysis) undergoes the HS ⇌ LS transition, while the other (*i.e.*, Fe(1)) remains in the HS state till 100 K.

The quantitative determination of the molar HS fraction γ_{HS} [$=A_{HS}/(A_{HS} + A_{LS})$] from the Mössbauer spectra was obtained based on the evolution of the area fractions A_{HS} and A_{LS} of the resonance lines.[19] The area fractions are proportional to the products $f_{HS} \cdot \gamma_{HS}$ and $f_{LS} \cdot \gamma_{LS}$, respectively, where γ and f are the molar fraction and Lamb–Mössbauer factor of the corresponding spin states.[38,39] The area fractions of the resonance signal in the Mössbauer spectra do not necessarily reflect the actual concentrations of the different iron spin states, as different bond strengths of the Mössbauer nuclide in its lattice position lead to different Lamb–Mössbauer factors, which in turn give rise to different intensities of the corresponding Mössbauer resonance signals. However, in the present analysis, we presumed identical Lamb–Mössbauer factors for the HS and LS states, where the HS and LS fractions just correspond to their area fractions A_{HS} and A_{LS}, respectively. Though in most of the cases $f_{HS} < f_{LS}$, the error involved in the assumption of f_{HS} =

f_{LS} is unlikely to be very high.[19] Thus, the value of γ_{HS} was obtained for the two temperatures of the study by directly relating the HS fraction to the area fraction of the doublets due to the HS species. The γ_{HS} value thus estimated at 100 K (≃0.5) is comparable with that obtained in the 180–30 K region from the magnetic studies (Fig. 4(b)). This result obtained from the Mössbauer spectroscopic study supplements the observations made from the magnetic studies as well as observations made from the crystal structure analysis. Thus, the results obtained from the magnetic and Mössbauer spectroscopic studies unequivocally establish that complex **1** under ambient pressure undergoes a thermally induced incomplete (half) spin transition [(HS + HS) ⇌ (HS + LS)] of Fe(II) at *ca.* 226 K and remains in the same (HS + LS) state till the lowest temperature of the study.

Origin of incomplete spin transition in 1

In search of the origin of the incomplete half-spin transition of Fe(II) in **1** and the reason why only Cation2 undergoes the transition, the crystal packing was analysed with attention to the π–π interactions between the bpp ligands as well as the degree of distortion. There are two crystallographically independent aryl–aryl π–π stacks as shown in Fig. 6 where one is between the bpp1 ligands while the other is between the bpp2 ligands. In both stacks only each edge of the pyrazolyl unit (C6–C7 for bpp1 and C16–C17 for bpp2) overlaps with each other, suggesting that the aryl–aryl interactions are considerably weak. Through the stacks, each of Cation1 and Cation2 forms a 1D π–π network along the *c* axis as shown in Fig. 6. The temperature-dependent interlayer distances are estimated as – bpp1–bpp1 = 3.253, 3.252, 3.304, and 3.297 Å, and bpp2–bpp2 = 3.225, 3.214, 3.193, and 3.184 Å at 300, 250, 200, and 100 K, respectively.

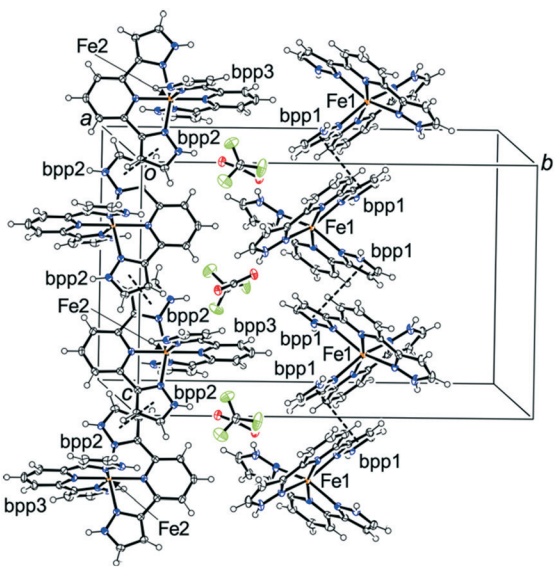

Fig. 6 View of the crystal structure of **1** at 100 K with π–π stacking as shown by dashed lines.

In contrast, the bpp3 ligands of Cation2 are free from any π–π stacking interactions, suggesting that they can move more freely than bpp1 and bpp2 ligands. Spin transition from the HS to LS state involves deformation and shrinkage, at which bpp3 of Cation2 will move more actively than bpp1 and bpp2 ligands. This appears to be the reason why Cation2 only shows the spin transition. A similar situation was observed in $[Fe(3\text{-bpp})_2][Cr(bpy)(ox)_2]_2$ containing both HS and LS Fe^{2+} cations in a 1:1 ratio.[40] The presence of π–π stacking interactions between the pyrazolyl units organized the dimers separated by a distance lying in the range 3.273(2)–3.490(4) Å.

As discussed above, the chemical environments of Cation1 and Cation2 are very similar but the degrees of distortion are significantly different. Halcrow *et al.*[41] derived some indices and put forward a relationship between those indices and the occurrence of spin transition in $[Fe(3\text{-bpp})_2]^{2+}$-based complexes. Table 3 shows such common indices estimated for **1**. Here, the angle α is an average of four internal N–Fe–N angles where the complexes with $72° < \alpha < 74°$ exhibit spin transition.[41] As shown in Table 3, the values of α for Cation1 and Cation2 fall well within this range. However, the value of α of Cation2 is a little more than the higher edge of this range, suggesting Cation2 as one of the least distorted complexes. The two other indices – the angle between two bpp ligands, θ and that on $N_{pyridine}$–Fe–$N_{pyridine}$, ϕ are also noted. It was proposed that all HS complexes remain in the HS state at all temperatures in the solid state if $\theta < 76°$ and/or $\phi < 172°$.[42] In this work, the observed values of θ (=69.32°) and ϕ(=167.04°) at 300 K for Cation1 (see Table 3) definitely satisfy the criteria so that Cation1 remains in the HS state in the whole temperature range of the study,[42] as is evident from the average of the Fe–N bond lengths (Table 2). On the other hand, the θ and ϕ values at 300 K for Cation2 are larger than those values, and therefore Cation2 can exhibit the spin transition behaviour.

In describing the degree of distortion from regular octahedral configuration, two parameters Σ and Θ are introduced. The first is the sum of the deviations from 90° of the average of 12 N–Fe–N angles (α_i), which is formulated as $\Sigma = \sum_{i=1}^{12} |90 - \alpha_i|$, whereas the second is the specific degree of trigonal distortion of the coordination geometry from an octahedron towards a trigonal prism given by $\Theta = \sum_{i=1}^{24} |60 - \beta_i|$, where β_i are the 24 torsion angles between adjacent N atoms on opposite triangular faces of the octahedron, measured along their common pseudo-three fold axis.[41,43] The results are collected in Table 3 together with other common indices. According to Halcrow *et al.*,[41,43] for a ST complex the values of Σ and Θ should lie in the $147 < \Sigma < 159°$ and $454 < \Theta < 480°$ ranges. As shown in Table 3, the values of Σ and Θ for Cation1 (161.8 and 535°) are on the upper edge and out of the predicted range, respectively, but those for Cation2 (145.22 and 467°) are near the lower edge and at the midpoint of the ranges predicted, respectively. This once again suggests that Cation2 is less distorted than

Table 3 Selected bond lengths (Å) and angular parameters (°) in the crystal structures of **1**[a]

	Cation1						Cation2					
T/K	300	250	200	100	$\Delta_{250-200\ K}$[c]	$\Delta_{300-100\ K}$[d]	300	250	200	100	$\Delta_{250-200\ K}$[c]	$\Delta_{300-100\ K}$[d]
d_{avg}/Å[b]	2.1708(19)	2.1683(17)	2.1715(18)	2.1741(16)	−0.0032	−0.0033	2.160(2)	2.1344(19)	1.9654(19)	1.9600(17)	0.1690	0.2000
α/°	73.93(8)	73.89(7)	73.94(7)	73.86(6)	−0.05	0.07	74.03(6)	74.53(6)	78.90(6)	79.06(5)	−4.37	−5.03
Σ/°	161.85(8)	163.57(7)	166.12(7)	168.33(6)	−2.55	−6.48	145.22(6)	140.32(6)	103.38(6)	104.18(5)	36.94	41.04
Θ/°	535.44	542.56	554.87	576.38	−12.31	−40.94	467.11	452.97	325.77	324.06	127.20	143.05
ϕ/°	167.04(11)	166.42(10)	165.39(10)	163.92(8)	1.03	3.12	180.0[e]	180.0[e]	180.0[e]	180.0[e]	0.0	0.0
θ/°	69.32	68.74	67.31	66.61	1.43	2.71	83.98	83.58	82.10	81.03	1.48	2.95

[a] α, Σ, and Θ are indices showing the spin state of **1**,[44,45] while θ and ϕ are indices showing whether the spin transition occurs or not.[44,45] Typical values for all of these parameters in high- and low-spin $[Fe(3\text{-bpp})_2]^{2+}$ derivatives are available in ref. 41. [b] Average of Fe–N distances. [c] Difference from 250 K to 200 K. [d] Difference from 300 K to 100 K. [e] The value is crystallographically fixed at 180°.

Cation1. The values of Σ and Θ for Cation1 indicate a large distortion, but the smaller θ and ϕ values bring in unfavourable conditions to occupy a LS state. The structural rearrangement required in **1** to make the θ and ϕ indices for Cation1 suitable (as per the range of values predicted[41,43]) for a LS state is too large to be accommodated by the 3D hydrogen-bonded rigid solid lattice.[41] On the other hand, Cation2 has definitely smaller values of Σ and Θ, suggesting that the degree of distortion of Cation2 is smaller than that of Cation1. The values of θ and ϕ for Cation2 are also slightly smaller than the range of predicted values.[41,43] Further, Cation2 has the smallest degree of distortion among the $[Fe(3\text{-bpp})_2]^{2+}$ complexes reported so far.[41]

Finally, we discuss the temperature dependence of the structures of Cation1 and Cation2. As stated above, Cation1 shows no ST behaviour in the whole temperature range. The indices corresponding to Cation1 estimated from 300 K to 100 K are almost similar (Table 3). With lowering of the temperature, the values of Σ and Θ decrease by 6.48° and 41°, respectively, suggesting slight release of distortion. On the other hand, with lowering of the temperature, the values of θ and ϕ decrease by 3.12° and 2.71°, respectively, though the values usually do not change before and after spin transition.[41] In addition, the octahedrally undistorted complex should have θ = 90° and ϕ = 180°. The larger deviations make the angular Jahn–Teller distortion of HS Fe(II) stable.[41] Therefore, these increases make the HS state more stable, which prevents Cation1 from changing its spin state to the LS state. Further, the average bond lengths of Fe–N measured at 300, 250, 200 and 100 K indicate that Cation2 is in the HS state at 300 and 250 K and is in the LS state at 200 and 100 K, respectively. Usually, LS states of Fe(II) have less distorted structures[41] as suggested by its electronic configuration $(t_{2g})^6$. Actually, with lowering of the temperature, the Σ and Θ values significantly decrease, suggesting that the LS state of Cation2 is less distorted than the HS state. The value of θ of Cation2 increases by 2.95° from 300 K to 100 K and the value of θ = 81.03° in the LS state is near and slightly less than the lower edge of the prescribed range (81.3–90.0°), which suggests that the LS state of Cation2 is more distorted than that found in normal $[Fe(3\text{-bpp})_2]^{2+}$-based ST complexes. In addition, the ϕ value of Cation2 has no temperature dependence as the N–Fe–N lies on a two-fold axis. The estimated values of $\Delta\Sigma$, $\Delta\Theta$, and $\Delta\theta$ are smaller than those reported so far.[44] Moreover, the value of Σ = 104.18° is out of the range of the LS state (80.1–96.1°).[41] Again, α = 79.06° is also on the lower edge of the reported range (79° < α < 81°), suggesting that Cation2 is more distorted than the reported complexes in the LS state.[41] Thus, with lowering of the temperature, Cation2 changes from a relatively less-distorted HS state to a more-distorted LS state. The present observations demonstrate that complex **1** exhibits the least structural change during spin transition as compared to $Fe(bpp)_2^{2+}$-based spin transition complexes reported so far owing to the strong 3D hydrogen bond network of **1** (Fig. 3) which does not favour large structural changes.

Conclusions

In conclusion, presently temperature-dependent single crystal X-ray diffraction, magnetization and ^{57}Fe Mössbauer spectroscopic studies are performed to understand the nature of the thermal HS ⇆ LS transition in the $[Fe(3\text{-bpp})_2](CF_3CO_2)_2$ complex. Structure analysis finds that only one of the two crystallographic Fe(II) sites undergoes the thermal spin transition not associated with any structural phase change. The magnetic study observes that the complex undergoes a transition from a full high-spin state at room temperature to a mixed spin (50% HS–50% LS) state making the spin transition incomplete. This is supplemented by the Mössbauer study which quantitatively detects the existence of HS Fe(II) sites at high temperatures and a mixed spin state at low temperatures. Further, the chemical environments of Cation1 and Cation2 are very similar but the degrees of distortions are significantly different. While discussing the temperature dependence of **1**, it is found that Cation1 shows no spin transition in the whole temperature range due to the stable HS Fe(II) state supported by angular Jahn–Teller distortion, while with decreasing temperature Cation2 moves from a relatively less-distorted HS state to a more-distorted LS state favoring the thermal spin transition giving rise to a mixed spin state below the spin transition temperature. Furthermore, the present complex exhibits the least structural change during spin transition as compared to $[Fe(3\text{-bpp})_2]^{2+}$-based complexes reported in the literature indicating a strong 3D hydrogen bond network.

As the LS state is favored at higher pressures or at very low temperatures,[34] a study on the effect of pressure on the course of spin transition in $[Fe(3\text{-bpp})_2](CF_3COO)_2$ attracted our attention to determine if a complete spin transition could be induced. Further, the counter anion plays an important role in determining the nature of spin transition in Fe(II) complexes, synthesis of another complex with trichloroacetate as a monovalent counteranion in place of trifluoroacetate attracts our attention.

Experimental

Synthesis of $[Fe(3\text{-bpp})_2](CF_3COO)_2$

The reagents used for synthesis – iron(II) sulfate heptahydrate, $FeSO_4{\cdot}7H_2O$, barium chloride dihydrate, $BaCl_2{\cdot}2H_2O$, sodium trifluoroacetate (CF_3COONa), and ethanol C_2H_5OH were purchased from Sigma Aldrich and were used without further purification. The bpp ligand was prepared by a literature method[45] using the direct reaction of *N*,*N*-dimethyl formamide dimethyl acetal with 2,6-diacetyl pyridine followed by the subsequent reaction of the enaminone intermediate with hydrazine hydrate.

The $[Fe(3\text{-bpp})_2](CF_3COO)_2$ complex in bulk was prepared from aqueous iron(II)sulphate heptahydrate (0.28 g, 1 mmol) with a slight excess of barium chloride dihydrate (0.27 g, 1.1 mmol) in 5 mL of water under an argon atmosphere. The reaction mixture was placed in a centrifuge for about 30 minutes. The clear solution containing iron(II) ions was decanted from the white barium sulphate precipitate using a syringe and the solution was reacted with a slight excess of 3-bpp (0.43 g, 2.2 mmol) in 20 mL warm ethanol. While the mixture was stirred under an argon atmosphere, the saturated aqueous solution of sodium trifluoroacetate (1 g) in 1 mL of water was added, whereupon the bright orange precipitate came out readily on reducing the volume while scratching. This was then filtered off, washed with a small amount of cold water and dried in air. A similar procedure, as described above, was adopted for the preparation of the single crystal of **1** where more excess bpp (0.85 g, 4.3 mmol) was used. The orange-brown single crystals were grown after the mixture was left at RT over a few days.

Elem. anal. calculated for $FeC_{26}H_{18}N_{10}O_4F_6$: C, 44.30; H, 2.56; N, 19.88. Found: C, 43.83; H, 2.93; N, 19.47.

The stability of the complex in the working range of temperatures was verified by thermogravimetric studies (Fig. S3†). At room temperature the complex has orange colour whereas it changes to dark brick red at 77 K (Fig. S5†).

Characterization

Single crystal X-ray diffraction data of **1** were collected with a Rigaku Rapid II imaging plate system (at 300 K and 100 K) and a Rigaku XtaLAB Synergy Custom (at 250 K and 200 K) with a MicroMax-007 HF/VariMax rotating-anode X-ray generator with confocal monochromatic Mo-K_α radiation. Data reduction, cell refinement, and absorption collection were performed using RAPID AUTO and CrysAlis, respectively. The structure was solved with SHELXT[46] and refined with SHELX2018[47] within CrystalStructure version 4.3.1. Powder X-ray diffraction data of the bulk sample were recorded using a Rigaku Miniflex 600 40 kW 15 mA benchtop diffractometer with Cu-K_α radiation in the 2–90° range. For calculation of Θ (the degree of trigonal distortion of the coordination geometry from an octahedron towards a trigonal prism) we used OctaDist 2.6.1 software.[48] Variable temperature magnetic measurements in the 10–300 K range were carried out using a Quantum Design MPMS2 magnetometer with twenty randomly oriented single crystals placed inside a thin plastic film as a holder. Necessary correction was made for the contribution from the sample holder. No difference in the magnetic data was obtained when measured with polycrystalline samples. ^{57}Fe Mössbauer spectra of **1** (single crystalline samples) were recorded using a conventional constant-acceleration spectrometer with a ^{57}Co Mössbauer source and a constant low temperature bath.

Conflicts of interest

There are no conflicts of interest to declare.

Acknowledgements

KHS, DO and HS gratefully acknowledge the support from the Institution of Research and Community Service, Yogyakarta State University (Agreement Contract: 85/Penelitian/WCR/

UN34.21/2019) and Mimin Aminah (ITB-Bandung) for the help in synthesis. AB expresses sincere thanks to Japan Society for the Promotion of Science (JSPS) for providing him a BRIDGE Fellowship to visit Osaka University, Japan, which gave him the chance to initiate this study.

Notes and references

1 P. Gütlich and H. A. Goodwin, in *Spin Crossover in Transition Metal Compounds I*, Springer, 2004, pp. 1–47.
2 M. A. Halcrow, *Spin-Crossover Materials: Properties and Applications*, John Wiley & Sons, 2013.
3 Q. M. Phung, A. Domingo and K. Pierloot, *Chem. – Eur. J.*, 2018, **24**, 5183–5190.
4 R. Torres-Cavanillas, R. Sanchis-Gual, J. Dugay, M. Coronado-Puchau, M. Giménez-Marqués and E. Coronado, *Adv. Mater.*, 2019, 1900039–1900044.
5 A. R. Craze, M. M. Bhadbhade, Y. Komatsumaru, C. E. Marjo, S. Hayami and F. Li, *Inorg. Chem.*, 2020, **59**, 1274–1283.
6 Z.-S. Yao, Z. Tang and J. Tao, *Chem. Commun.*, 2020, **56**, 2071–2086.
7 H. Hagiwara, R. Minoura, T. Udagawa, K. Mibu and J. Okabayashi, *Inorg. Chem.*, 2020, **59**, 9866–9880.
8 A. Enriquez-Cabrera, A. Rapakousiou, M. P. Bello, G. Molnár, L. Salmon and A. Bousseksou, *Coord. Chem. Rev.*, 2020, **419**, 213396–213418.
9 V. Jornet-Mollá, C. Giménez-Saiz, L. Cañadillas-Delgado, D. S. Yufit, J. A. K. Howard and F. M. Romero, *Chem. Sci.*, 2021, **12**, 1038–1053.
10 A. Y. Verat, N. Ould-Moussa, E. Jeanneau, B. Le Guennic, A. Bousseksou, S. A. Borshch and G. S. Matouzenko, *Chem. – Eur. J.*, 2009, **15**, 10070–10082.
11 M. C. Young, E. Liew, J. Ashby, K. E. McCoy and R. J. Hooley, *Chem. Commun.*, 2013, **49**, 6331–6333.
12 B. Weber, W. Bauer, T. Pfaffeneder, M. M. Dîrtu, A. D. Naik, A. Rotaru and Y. Garcia, *Eur. J. Inorg. Chem.*, 2011, 3193–3206.
13 H. A. Goodwin and K. H. Sugiyarto, *Chem. Phys. Lett.*, 1987, **139**, 470–474.
14 K. H. Sugiyarto and H. A. Goodwin, *Aust. J. Chem.*, 1988, **41**, 1645–1663.
15 K. Sugiyarto and H. Goodwin, *Aust. J. Chem.*, 1994, **47**, 263–277.
16 T. Buchen, P. Gütlich, K. H. Sugiyarto and H. A. Goodwin, *Chem. – Eur. J.*, 1996, **2**, 1134–1138.
17 K. H. Sugiyarto, K. Weitzner, D. C. Craig and H. A. Goodwin, *Aust. J. Chem.*, 1997, **50**, 869–873.
18 K. H. Sugiyarto, M. L. Scudder, D. C. Craig and H. A. Goodwin, *Aust. J. Chem.*, 2000, **53**, 755–765.
19 A. Bhattacharjee, V. Ksenofontov, K. H. Sugiyarto, H. A. Goodwin and P. Gütlich, *Adv. Funct. Mater.*, 2003, **13**, 877–882.
20 K. H. Sugiyarto, W. A. McHale, D. C. Craig, A. D. Rae, M. L. Scudder and H. A. Goodwin, *Dalton Trans.*, 2003, 2443–2448.
21 A. Bhattacharjee, J. Kusz, V. Ksenofontov, K. H. Sugiyarto, H. A. Goodwin and P. Gütlich, *Chem. Phys. Lett.*, 2006, **431**, 72–77.
22 G. A. Craig, O. Roubeau and G. Aromí, *Coord. Chem. Rev.*, 2014, **269**, 13–31.
23 L. J. Kershaw Cook, R. Kulmaczewski, S. A. Barrett and M. A. Halcrow, *Inorg. Chem. Front.*, 2015, **2**, 662–670.
24 Z. Y. Li, Y. X. Wang, J. Zhu, S. Q. Liu, G. Xin, J. J. Zhang, H. Q. Huang and C. Y. Duan, *Cryst. Growth Des.*, 2013, **13**, 3429–3437.
25 V. Jornet-Mollá, Y. Duan, C. Giménez-Saiz, Y. Tang, P. Li, F. M. Romero and R. Xiong, *Angew. Chem.*, 2017, **129**, 14240–14244.
26 M. Attwood, H. Akutsu, L. Martin, D. Cruickshank and S. S. Turner, *Dalton Trans.*, 2019, **48**, 90–98.
27 V. Jornet-Mollá, C. Giménez-Saiz and F. M. Romero, *Crystals*, 2018, **8**, 1–13.
28 G. A. Craig, J. Sánchez Costa, O. Roubeau, S. J. Teat and G. Aromí, *Chem. – Eur. J.*, 2011, **17**, 3120–3127.
29 L. A. Barrios, E. Peyrecave-Lleixà, G. A. Craig, O. Roubeau, S. J. Teat and G. Aromí, *Eur. J. Inorg. Chem.*, 2014, **2014**, 6013–6021.
30 K. H. Sugiyarto, C. Kusumawardani, H. Sutrisno and M. W. A. Wibowo, *Orient. J. Chem.*, 2018, **34**, 735–742.
31 H. A. Goodwin, E. S. Kucharski and A. H. White, *Aust. J. Chem.*, 1983, **36**, 1115–1124.
32 P. J. Van Koningsbruggen, Y. Garcia, H. Kooijman, A. L. Spek, J. G. Haasnoot, O. Kahn, J. Linares, E. Codjovi and F. Varret, *J. Chem. Soc., Dalton Trans.*, 2001, 466–471.
33 A. Bhattacharjee, V. Ksenofontov, J. A. Kitchen, N. G. White, S. Brooker and P. Gütlich, *Appl. Phys. Lett.*, 2008, **92**, 174104–174107.
34 A. Bhattacharjee, M. Roy, V. Ksenofontov, J. A. Kitchen, S. Brooker and P. Gütlich, *Eur. J. Inorg. Chem.*, 2013, 843–849.
35 E. A. Boudreaux and L. N. Mulay, *Theory and Applications of Molecular Paramagnetism*, John Wiley & Sons, 1976.
36 T. Buchen, P. Gütlich and H. Toftlund, *Chem. – Eur. J.*, 1996, **2**, 1129–1133.
37 A. Bhattacharjee, P. J. Van Koningsbruggen, J. S. Miller and P. Gütlich, *J. Phys. Chem. Solids*, 2008, **69**, 2713–2718.
38 E. König, G. Ritter and H. A. Goodwin, *Chem. Phys.*, 1974, **5**, 211–223.
39 J. Jung, H. Spiering, Z. Yu and P. Gütlich, *Hyperfine Interact.*, 1995, **95**, 107–128.
40 M. Clemente-León, E. Coronado, M. C. Giménez-López and F. M. Romero, *Inorg. Chem.*, 2007, **46**, 11266–11276.
41 M. A. Halcrow, *Coord. Chem. Rev.*, 2009, **253**, 2493–2514.
42 L. J. Kershaw Cook, F. L. Thorp-Greenwood, T. P. Comyn, O. Cespedes, G. Chastanet and M. A. Halcrow, *Inorg. Chem.*, 2015, **54**, 6319–6330.
43 M. Marchivie, P. Guionneau, J.-F. Létard and D. Chasseau, *Acta Crystallogr., Sect. B: Struct. Sci.*, 2005, **61**, 25–28.
44 M. A. Halcrow, *Chem. Soc. Rev.*, 2011, **40**, 4119–4142.
45 Y. Lin and S. A. Lang Jr, *J. Heterocycl. Chem.*, 1977, **14**, 345–347.
46 G. M. Sheldrick, *Acta Crystallogr., Sect. A: Found. Adv.*, 2015, **71**, 3–8.
47 G. M. Sheldrick, *Acta Crystallogr., Sect. C: Struct. Chem.*, 2015, **71**, 3–8.
48 R. Ketkaew, Y. Tantirungrotechai, P. Harding, G. Chastanet, P. Guionneau, M. Marchivie and D. J. Harding, *Dalton Trans.*, 2021, **50**, 1086–1096.